SCIENCE CHINA
Information Sciences

• LETTER •

December 2023, Vol. 66 229405:1–229405:2
https://doi.org/10.1007/s11432-022-3749-3

Nonlinear neural computation in an integrated FP-SA spiking neuron subject to incoherent dual-wavelength optical pulse injections

Ziwei SONG[1], Shuiying XIANG[1*], Xingxing GUO[1], Shuang GAO[1], Biling GU[1], Dianzhuang ZHENG[1,2], Xiangfei CHEN[3] & Yuechun SHI[2*]

[1]*State Key Laboratory of Integrated Service Networks, State Key Discipline Laboratory of Wide Bandgap Semiconductor Technology, Xidian University, Xi'an* 710071*, China;*
[2]*Yongjiang Laboratory, Ningbo* 315202*, China;*
[3]*Key Laboratory of Intelligent Optical Sensing and Manipulation, Ministry of Education, National Laboratory of Solid State Microstructures, College of Engineering and Applied Sciences, Institute of Optical Communication Engineering, Nanjing University, Nanjing* 210023*, China*

Received 9 October 2022/Revised 15 January 2023/Accepted 20 April 2023/Published online 2 November 2023

Citation Song Z W, Xiang S Y, Guo X X, et al. Nonlinear neural computation in an integrated FP-SA spiking neuron subject to incoherent dual-wavelength optical pulse injections. Sci China Inf Sci, 2023, 66(12): 229405, https://doi.org/10.1007/s11432-022-3749-3

Photonic nonlinear computation is the critical cornerstone of photonic neuromorphic computing. As one of the key information function units in the photonic spiking neural networks, the photonic spiking neurons are responsible for the nonlinear computation of the network. Recently, the neuron-like nonlinear computation of the photonic spiking neuron has attracted considerable attention. Numerous photonic spiking neuron models based on different systems have been proposed, including phase change materials (PCMs) [1], resonant tunneling diodes [2], and various types of semiconductor lasers. Compared to these neuron models, a photonic spiking neuron chip based on a Fabry-Pérot laser with a saturable absorber (FP-SA) [3] has inherent advantages, such as easier fabrication, a higher output power, a faster response speed, easy control with gain current and reverse voltage, making it a reconfigurable and programmable spiking neuron. The previous work [4] reported the neuron-like dynamics of an FP-SA laser subjected to a single-wavelength optical pulse injection. Given the multi-longitudinal mode characteristic of the FP-SA laser, the neuron-like response of FP-SA lasers injected with the light of different wavelengths deserves further investigation. Incoherent wavelength optical injections come from multiple different light sources, reducing the optical power requirement of a single light source, which is beneficial to implement large-scale networks.

In this study, neuron-like nonlinear computations in an FP-SA photonic spiking neuron chip subjected to dual-wavelength optical pulse injections are experimentally demonstrated. Specifically, the FP-SA neuron achieves the spike threshold, temporal integration, and refractory period responses, and the wavelength conditions of two branch injection lights that lead to successful neuron-like behaviors are revealed.

Experiment. The experimental setup based on an all-fiber-optic system is shown in Figure 1(a), where two incoherent lights are injected into an FP-SA laser. Lights from two TLs (AQ2200-136 TLS module) with distinct wavelengths (λ_{in1} and λ_{in2}) are intensity-modulated using Mach-Zehnder modulators (MZM1 and MZM2). Here, two MZMs are respectively modulated by two radio frequency (RF) signals from an arbitrary waveform generator (AWG, Tektronix AWG70001B). The RF signals are respectively amplified using RF amplifiers (RF PA1 and RF PA2) before entering two MZMs. Here, two TLs' outputs are respectively polarization matched to two MZMs using polarization controllers (PC1 and PC2). Then, the modulated signal from MZM1 is passed through a variable optical delay line (VODL) and is combined with the modulated signal from MZM2 by a 50:50 optical coupler (OC1). The role of VODL is to compensate for the delay between two optical paths. Following that, the power of the resultant modulated signal is adjusted using a variable optical attenuator (VOA), and this signal is polarization matched to the FP-SA using PC3. After passing through the 10:90 OC2 and an optical circulator (CIRC), the modulated signal is injected into the facet of the gain section of the FP-SA. Here, the 10% branch of OC2 is used to monitor the injection power using a power meter (PM). The FP-SA output passes again through the CIRC into the 50:50 OC3 for analysis using a photodetector (PD, Agilent/HP 11982A), a real-time oscilloscope (SCOPE, Keysight DSOV334A), and an optical spectrum analyzer (OSA, Advantest Q8384).

The FP-SA laser chip includes a gain region and a sat-

* Corresponding author (email: jxxsy@126.com, yuechun-shi@ylab.ac.cn)

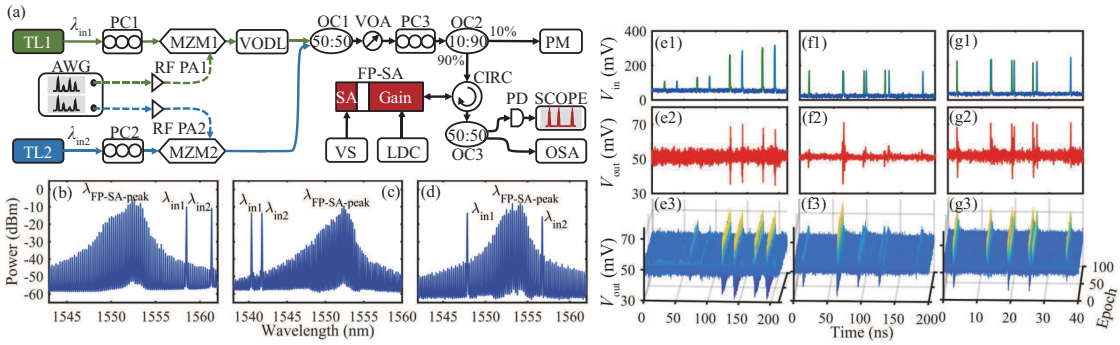

Figure 1 (Color online) (a) Diagram of the experimental setup. (b) The optical spectra of the FP-SA neuron when two signals are both injected into the right side of $\lambda_{\text{FP-SA-peak}}$. (c) The optical spectra of the FP-SA neuron when two signals are both injected into the left side of $\lambda_{\text{FP-SA-peak}}$. (d) The optical spectra of the FP-SA neuron when two signals are injected into different sides of $\lambda_{\text{FP-SA-peak}}$. The total modulated signal injected into the FP-SA neuron for (e1) the threshold response, (f1) the temporal integration response, and (g1) the refractory period response. (e2) The threshold response of the FP-SA neuron. (e3) A three-dimensional color graph of the threshold response of 100 epochs. (f2) The temporal integration response of the FP-SA neuron. (f3) A three-dimensional color graph of the temporal integration response of 100 epochs. (g2) The refractory period response of the FP-SA neuron. (g3) A three-dimensional color graph of the refractory period response of 100 epochs.

urable absorber (SA) region. A laser diode controller (LDC, ILX Lightwave LDC3724B) provides a low-noise bias current and precise temperature control for the gain region. The voltage source (VS) is used to reverse bias the SA. In this work, the SA length of the FP-SA laser chip is 90 μm, and the peak wavelength is denoted as $\lambda_{\text{FP-SA-peak}}$. In the experiment, three categories of wavelength schemes are considered. As the optical spectrum shown in Figure 1(b), the first case is that the modulated signals from TL1 and TL2 are both injected into the right side of $\lambda_{\text{FP-SA-peak}}$. As presented in Figure 1(c), the second case is that two modulated signals are both injected into the left side of $\lambda_{\text{FP-SA-peak}}$. The third case is that two signals are injected into different sides of $\lambda_{\text{FP-SA-peak}}$ as displayed in Figure 1(d).

Results and discussion. Taking the first injection case shown in Figure 1(b) as an example, Figures 1(e)–(g) demonstrate neuron-like nonlinear computation of the FP-SA neuron subject to incoherent dual-wavelength optical pulse injections, including spike threshold, temporal integration, and refractory period. Herein, Figures 1(e1), (f1), and (g1) present the injection signals specially designed by AWG, where green and blue spikes respectively represent the modulated signals from TL1 and TL2. The nonlinear response results are illustrated in Figures 1(e2), (f2), and (g2). To verify the reproducibility of the experiment, Figures 1(e3), (f3), and (g3) plot three-dimensional color graphs of the FP-SA responses to 100 consecutive external stimuli.

As shown in Figure 1(e2), the third and the fourth pairs of injection pulses trigger the FP-SA to generate neuron-like spikes, while there is no response when the first and the second pairs of injection pulses are injected the FP-SA, which shows once the injection power exceeds the excitability threshold, the FP-SA neuron can be excited.

The temporal integration effect of the FP-SA neuron is illustrated in Figure 1(f2). The first pulse pair with the minimal inter-spike interval (ISI) triggers a spike generation of the FP-SA neuron, while the pulse pairs with larger ISIs do not elicit the response spikes. Meanwhile, the first single pulse from TL1 and the last single pulse from TL2 both fail to trigger a spike, indicating that a single pulse cannot reach the spike threshold. It means that the two closely spaced pulses with different wavelengths are temporally integrated and thus exceed the threshold.

By increasing the injection power, the refractory period of the FP-SA neuron is observed. As shown in Figure 1(g2), the first single pulse and the last single pulse can both elicit a spike response, indicating that the single perturbation pulse power exceeds the threshold. For the last two pulse pairs with larger ISIs, each injection pulse can trigger a spike. However, for the first pulse pairs, the first injection pulse triggers a spike, while the second injection pulse fails to elicit another spike response, demonstrating the existence of the refractory period.

Similarly, the aforementioned spike threshold, temporal integration, and refractory period are also implemented in the other two wavelength schemes shown in Figures 1(c) and (d). These results reveal that two external injection signals of arbitrary wavelengths aligned with the longitudinal modes of the FP-SA can successfully perform neuron-like nonlinear computations. Moreover, the proposed incoherent wavelength optical injection scheme of an FP-SA can reduce the optical power requirement of the optical source, which is in favor of constructing large-scale incoherent photonic spiking neural networks.

Acknowledgements This work was supported in part by National Key Research and Development Program of China (Grant Nos. 2021YFB2801900, 2021YFB2801901, 2021YFB2801902, 2021YFB2801903, 2021YFB2801904, 2018YFE0201200), National Outstanding Youth Science Fund Project of National Natural Science Foundation of China (Grant No. 62022062), National Natural Science Foundation of China (Grant Nos. 61974177, 61674119), and Fundamental Research Funds for the Central Universities (Grant No. QTZX23041).

References

1 Feldmann J, Youngblood N, Wright C D, et al. All-optical spiking neurosynaptic networks with self-learning capabilities. Nature, 2019, 569: 208–214
2 Romeira B, Javaloyes J, Ironside C N, et al. Excitability and optical pulse generation in semiconductor lasers driven by resonant tunneling diode photo-detectors. Opt Express, 2013, 21: 20931–20940
3 Xiang S Y, Shi Y C, Guo X X, et al. Hardware-algorithm collaborative computing with photonic spiking neuron chip based on an integrated Fabry-Perot laser with a saturable absorber. Optica, 2023, 10: 162–171
4 Zheng D Z, Xiang S Y, Guo X X, et al. Experimental demonstration of coherent photonic neural computing based on a Fabry-Perot laser with a saturable absorber. Photon Res, 2023, 11: 65–71